Electronic Supplementary Material (ESI) for Materials Chemistry Frontiers.

Supplementary Information

Metal–Organic Frameworks Mediated Synthesis of Bell String-like Hollow ZnS-C Nanofibers to Enhance Sodium Storage Performance

Xianbin Wei, Haocheng Yuan, Haijun Wang, Ruoqian Jiang, Jinle Lan, * Yunhua Yu, *

Xiaoping Yang

State Key Laboratory of Organic-Inorganic Composites, College of Materials Science and Engineering, Beijing University of Chemical Technology, Beijing 100029, China

*Corresponding author: lanjl@mail.buct.edu.cn; yuyh@mail.buct.edu.cn

1 Materials Characterization.

Crystalline structures of the as-prepared different samples were investigated by A wide-angle X-ray diffraction (WAXD, D8 Advance, Bruker, Cu Kα, λ=0.154 nm). And the Raman spectra analysis were performed via INVIA Reflex apparatus. The surface characteristics which included the specific surface area and porosity distribution were investigated by Brunauer-Emmett-Teller (BET) analyzers (Micrmeritics, ASAP 2020), and the pore diameter distribution were analyzed via density functional theory (DFT) calculation model. The morphology and microstructure were explored by a field emission scanning electron microscope (FE-SEM, HITACHI S-4700) and high-resolution transmission electron microscope (HR-TEM, JEM-3013, JEOL). The thermal weight loss was measured by a thermogravimetric analysis (TGA) with the instrument (TGA/DSC3+, Switzerland, 10 ℃ min^{-1}, Air). The elemental composition and chemical status of the as-prepared samples were characterized by X-ray photoelectron spectroscopy (XPS, ESCALAB 250, Thermo Scientific K-Alpha^{+}) with monochromatic Al X ray as the excitation source. Fourier transform infrared spectra (FT-IR) were measured with Nicolet 6700 infrared spectroscopy instrument. The UV-vis spectra were tested by Shimadzu UV-2550 spectrophotometer.

2 Preparation of Na_2S_6 solution.

To prepare Na_2S_6 solution, the S powders and Na_2S mixture with a molar ratio of 5:1 were dissolved into moderate 1,2-dimethoxyethane (DME) by stirring for two days. And the solution needed to be further diluted before using.

3 Electrochemical measurement.

The electrochemical performance of the CNFs, ZnS nanoparticles and ZnS@CNFs were tested in CR 2032 coin-type cells. The CNFs and ZnS@CNFs films were directly pouched into discs of 12 mm diameter (mass loading is about 0.8-1.2 mg cm^{-1}) as free-standing anodes. The ZnS@C-800 nanoparticles derived from ZIF-8 were mixed with Super P and sodium carboxymethylcellulose (CMC) in a ratio of 8:1:1. Then the obtained slurry was coated on the copper foil and vacuum-dried at 80 ℃ for 24 h. The $Na_3V_2(PO_4)_3$ (NVP) powders were purchased from WuXi Kai-Star Electro-optic Materials Co., Ltd. The cathode slurry was prepared via mixing the powders, Super P and polyvinylidene fluoride in a ratio of 8:1:1, and adequate volume of N-methylpyrrolidone (NMP) was used as the solvent. After that, the obtained slurry was coated on the aluminum foil and vacuum-dried at 120 ℃ for 12 h.

All the electrolyte-related chemicals were purchased from Dodochem without further purification. The applied electrolyte was 1 M NaF_6 dissolved in DME with a Whatman glass fiber membrane as the separator. The half-cells were assembled in an argon-filed glovebox with metallic sodium as the reference electrode. The full-cells were assembled with 1.5-ZnS@CNFs-800 free-standing anodes and NVP cathodes in the N/P ratio of 1.05:1. Before assembling the full-cells, the 1.5-ZnS@CNFs-800 anodes were pre-sodiated by cycling for 5 cycles at 0.1 A g^{-1} in the half-cells. The galvanostatic charge-discharge (GCD) experiments were tested between 0.005 and 4.2 V.

The rate and cycle performance of the as-assembled coin cells were measured with Land CT2001 battery tester. CV measurement (0.005-3 V, vs Na/Na^+) at different scan rates and EIS (0.01-10^7 Hz) were tested on an AutoLab PGSTAT 302 N workstation.

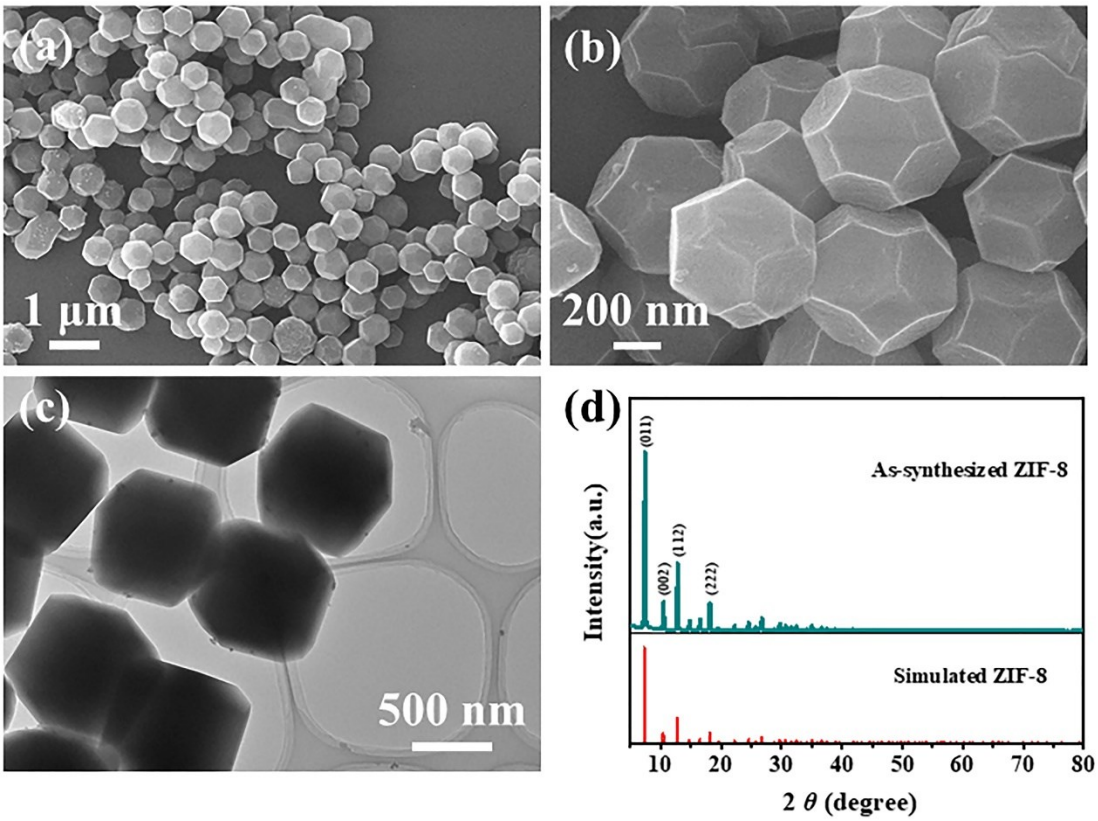

Fig. S1 (a) and (b) SEM images, (c) TEM image and (d) XRD pattern of zeolitic imidazolate framework 8 (ZIF-8).

The ZIF-8 was prepared according to the previous reported method and further optimized.[1]

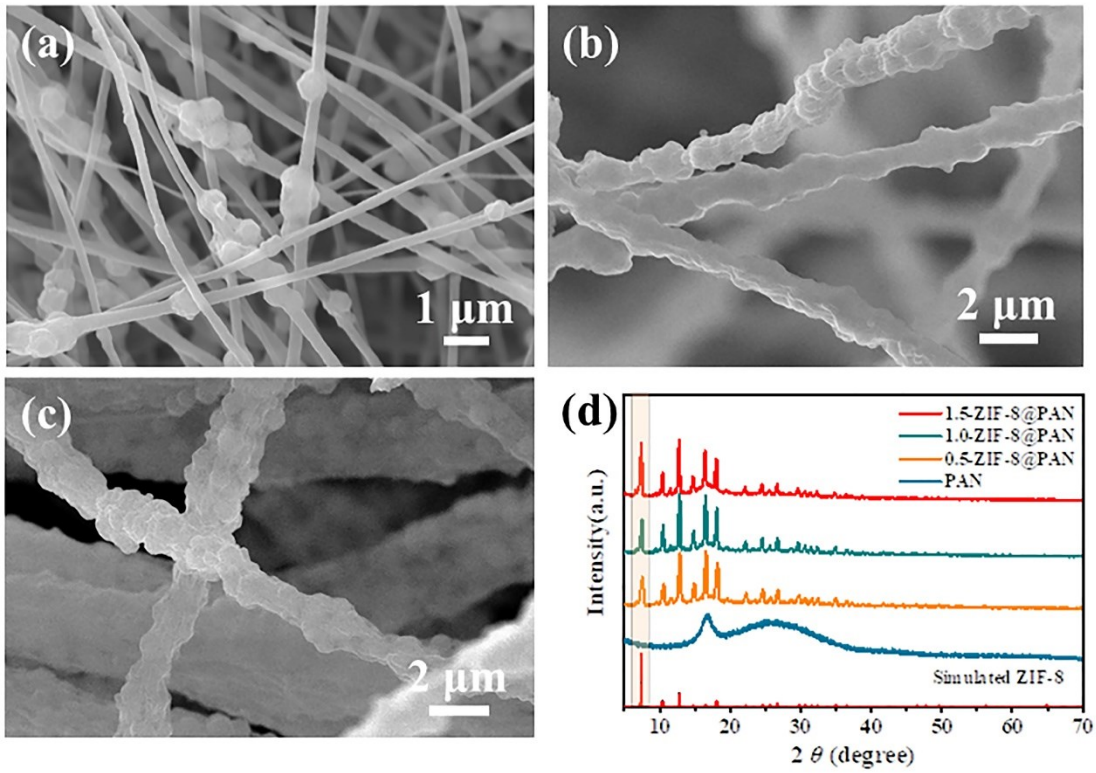

Fig. S2 SEM images of (a) 0.5-ZIF-8@PAN nanofibers, (b) 1.0-ZIF-8@PAN nanofibers and (c) 1.5-ZIF-8@PAN nanofibers. (d) XRD patterns of various composites films.

As shown in Figure S2, ZIF-8 could be uniformly distributed and gradually filled up the PAN nanofiber as the mass ratio of ZIF-8 to PAN increased from 0.5 to 1.5. When the mass ratio was higher than 1.5, it was very difficult to operate the electrospinning due to high viscosity of solution and difficulty in dispersion.

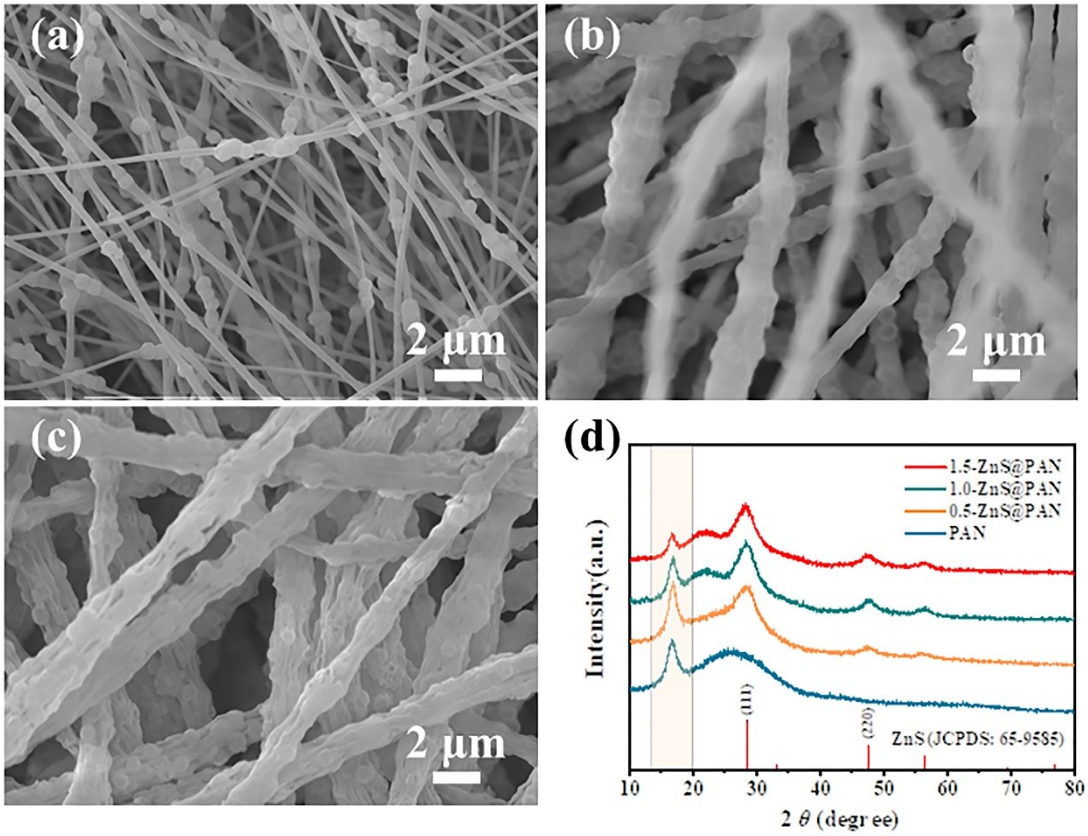

Fig. S3 SEM images of (a) 0.5-ZnS@PAN nanofibers, (b) 1.0-ZnS@PAN nanofibers and (c) 1.5-ZnS@PAN nanofibers. (d) XRD patterns of various composites films.

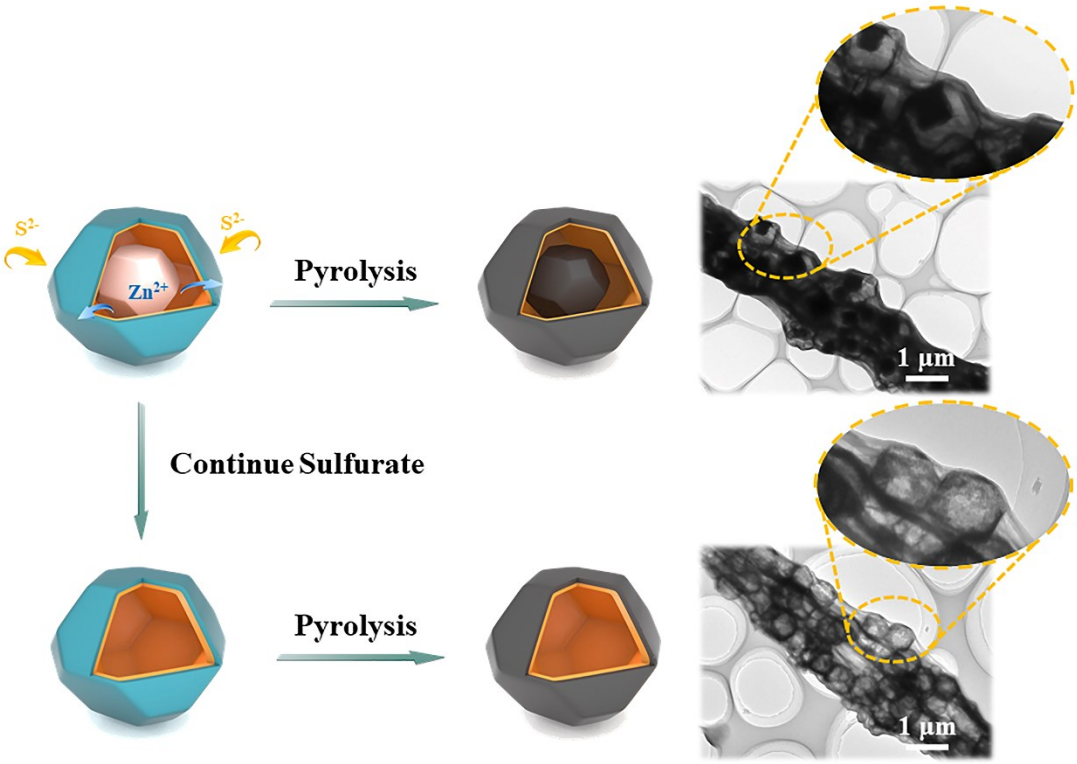

Fig. S4 Synthetic scheme for the evolution of hollow ZnS.

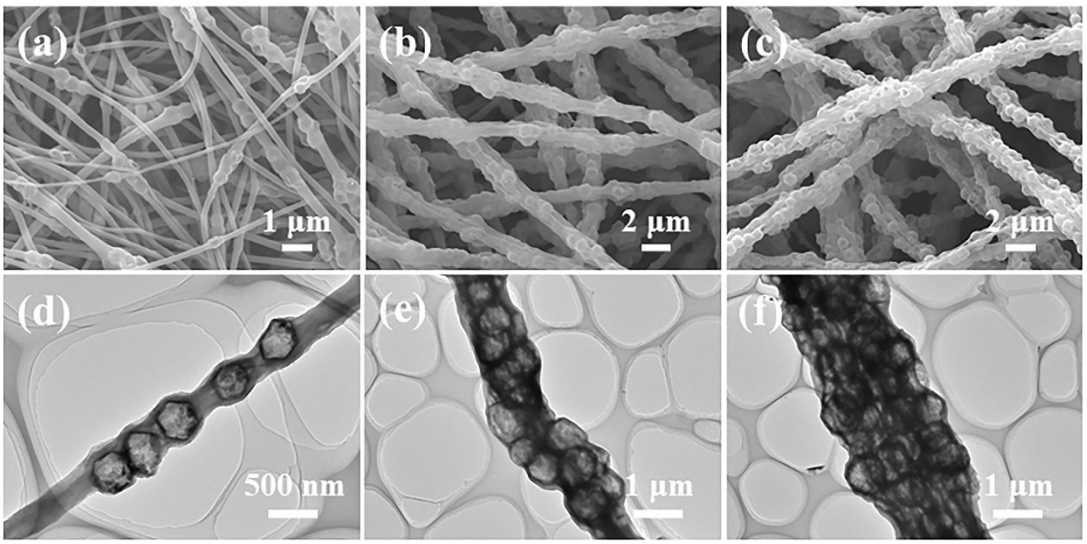

Fig. S5 SEM and TEM images of (a, d) 0.5-ZnS@CNFs-800, (b, e) 1.0-ZnS@CNFs-800, and (c, f) 1.5-ZnS@CNFs-800.

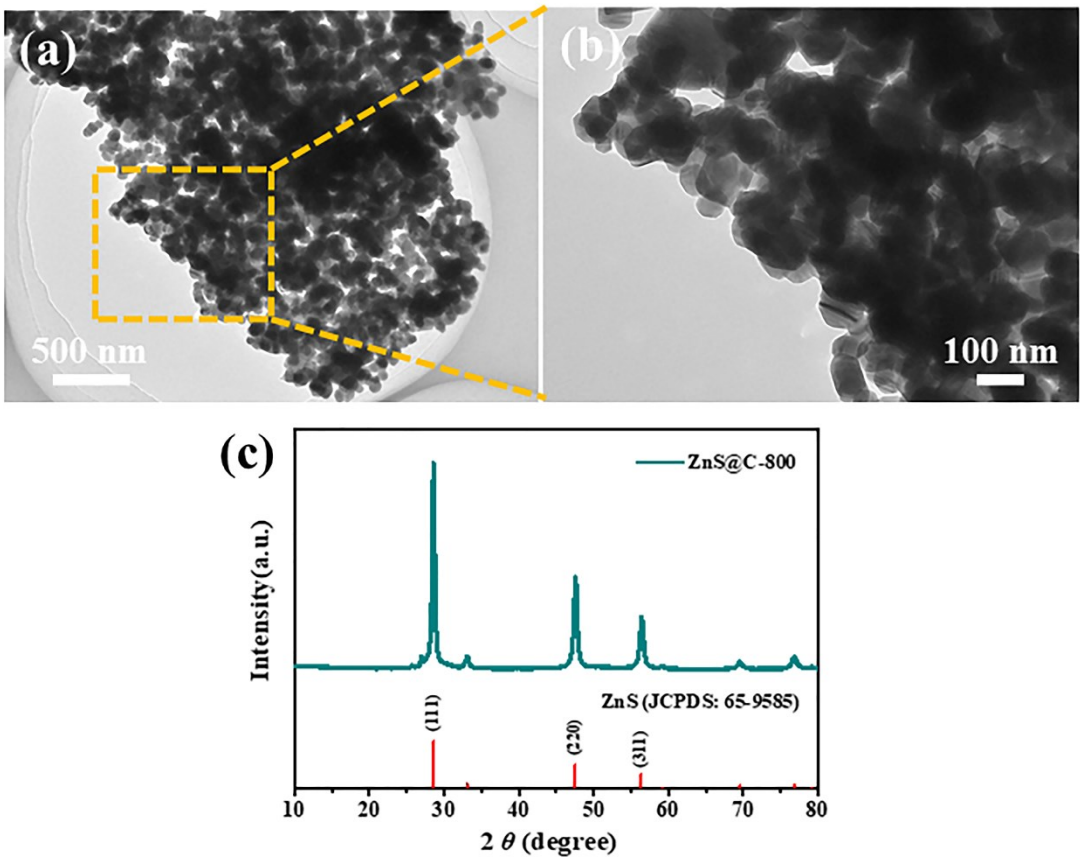

Fig. S6 (a, b) TEM images and (c) XRD pattern of as-prepared ZnS@C-800.

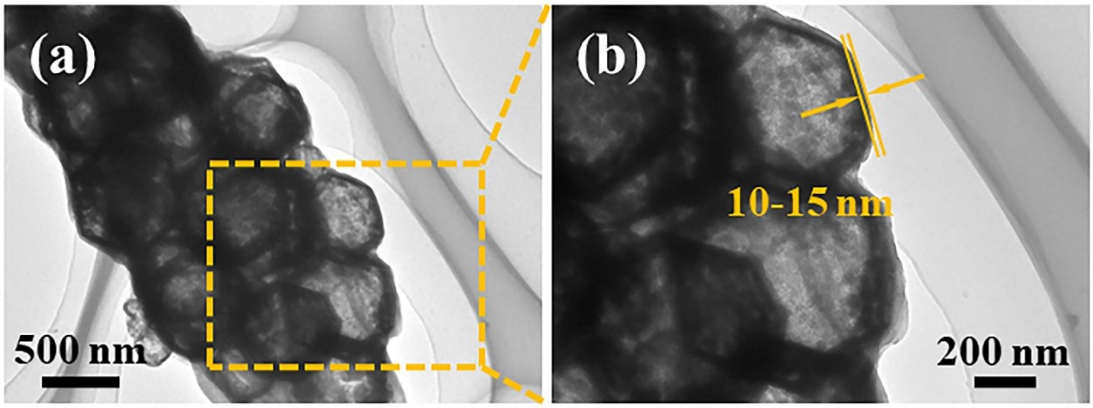

Fig. S7 TEM images of 1.5-ZnS@CNFs-800 to identify the thickness of carbon shells.

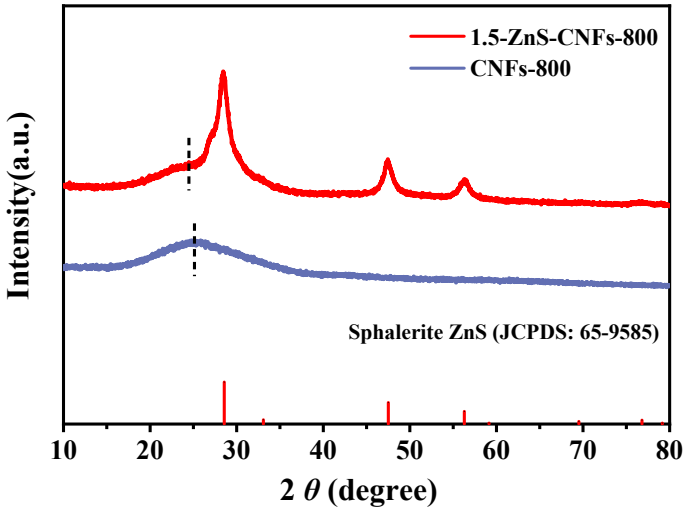

Fig. S8 XRD patterns of 1.5-ZnS@CNFs-800 and CNFs-800.

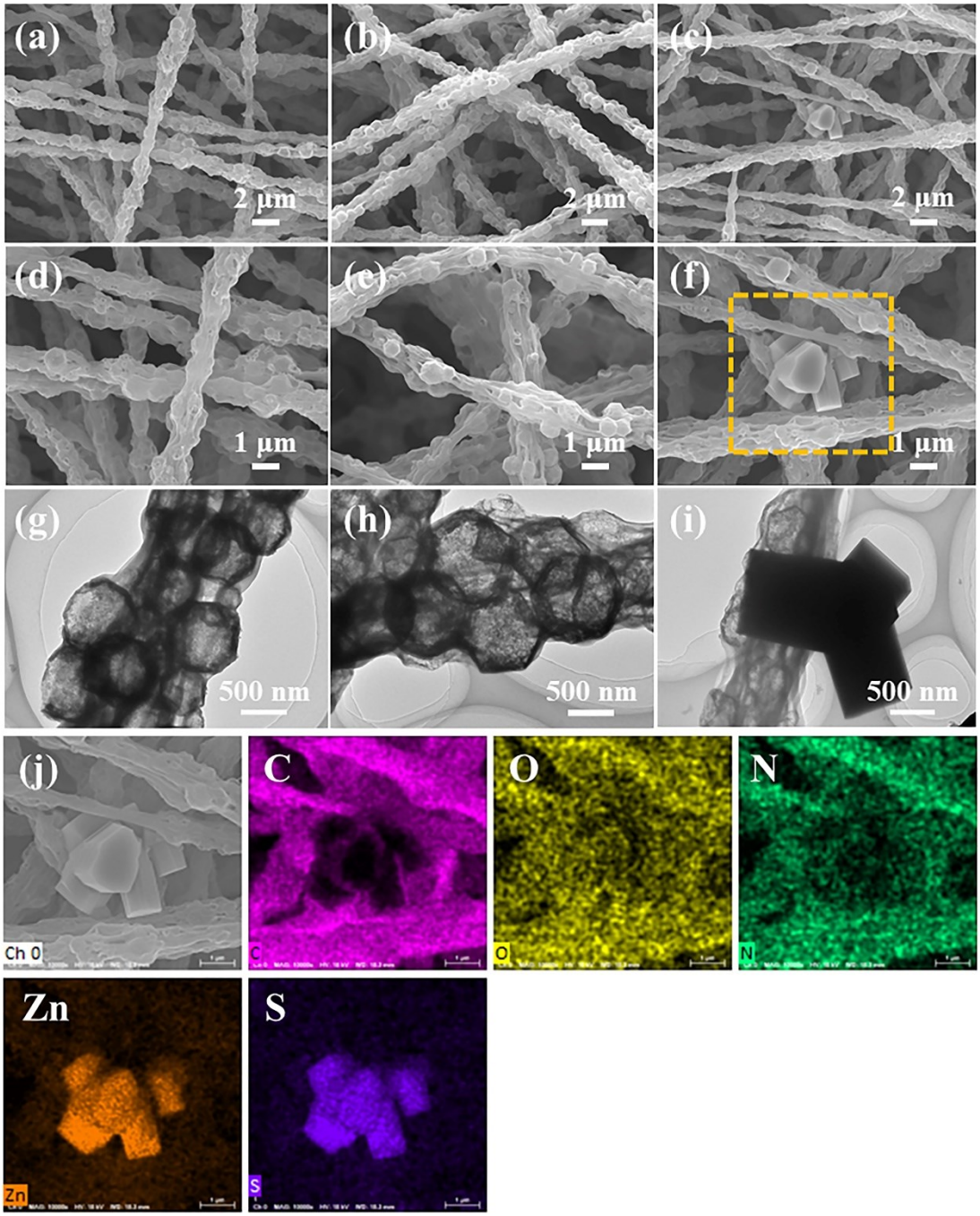

Fig. S9 SEM and TEM images of (a, d, g) 1.5-ZnS@CNFs-700, (b, e, h) 1.5-ZnS@CNFs-800, and (c, f, i) 1.5-ZnS@CNFs-900. (j) Element distribution of C, O, N, Zn and S for 1.5-ZnS@CNFs-900 composite.

Compared with the other two composites at 700℃ and 800℃, the inner ZnS particles separate from the nanofiber surface and transform into more stable wurtzite phase of bulk ZnS when carbonized at 900℃.

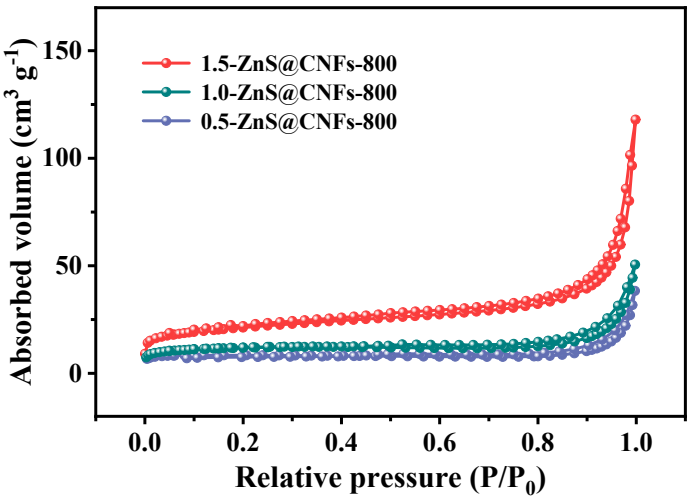

Fig. S10 N_2 adsorption-desorption isotherms of 0.5, 1.0, and 1.5-ZnS@CNFs-800 composites.

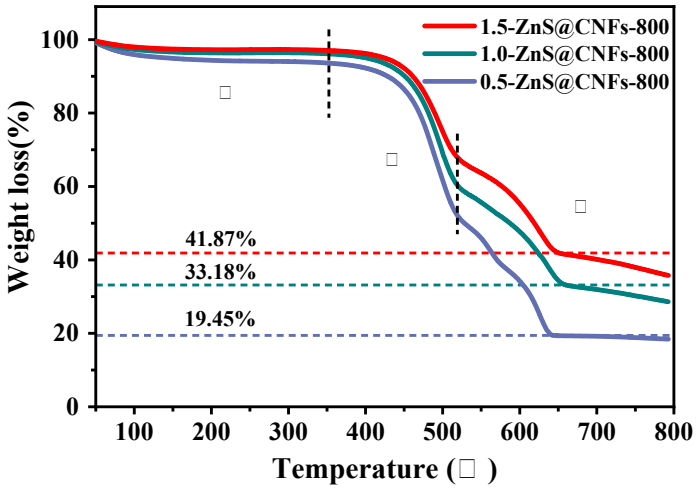

Fig. S11 Thermal gravimetric curves of 0.5, 1.0 and 1.5-ZnS@CNFs-800 composites.

For the ZnS@CNFs electrode, there are three weightlessness processes during the pyrolysis at air atmosphere as following:

Step I: (0-350 ℃) Evaporation of absorbed water

Step II: (350-520 ℃) Conbustion of carbon

Step III: (520-650 ℃) Conversion of ZnS to ZnO

And the corresponding physical or chemical reactions are:

$$H_2O(l) \rightarrow H_2O(g)$$

$$C(s) + O_2(g) \rightarrow CO_2(g)$$

$$ZnS(s) + O_2(g) \rightarrow ZnO(s) + SO_2(g)$$

Based on the TGA measurement curves, the residual component when they are heated to 650 ℃ is ZnO. According to the conservation of Zn element, the mass percentage of ZnS in the sample can be calculated in line with the formula: ZnS % = ZnO %×1.196. The ZnS contents of 0.5, 1.0, and 1.5-ZnS@CNFs-800 samples can be calculated as 23.3 %, 39.7 %, and 50.1 %, respectively.

According to the theoretical capacity of ZnS (≈ 550 mA h g^{-1})[2] and CNFs (≈ 200 mA h g^{-1}),[3] the theoretical capacity of 0.5-ZnS@CNFs-800, 1.0-ZnS@CNFs-800 and 1.5-ZnS@CNFs-800 are about 281.55 mA h g^{-1}, 338.95 mA h g^{-1} and 375.35 mA h g^{-1}.

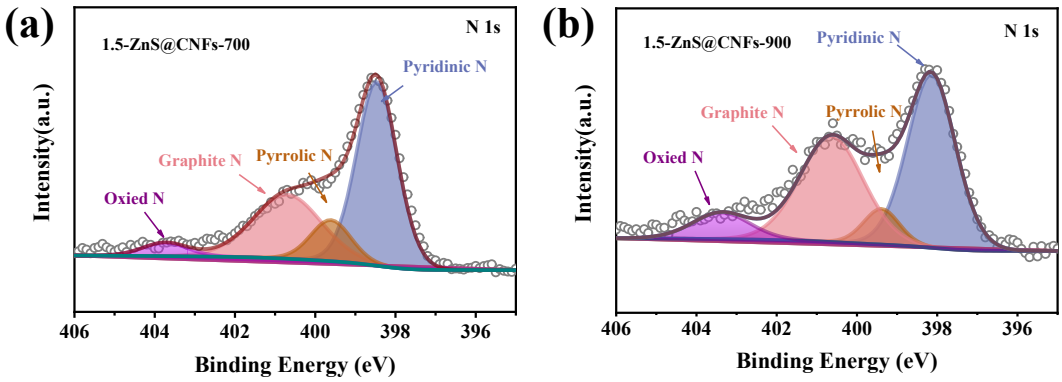

Fig. S12 XPS N 1s spectra of (a) 1.5-ZnS@CNFs-700 and (b) 1.5-ZnS@CNFs-900.

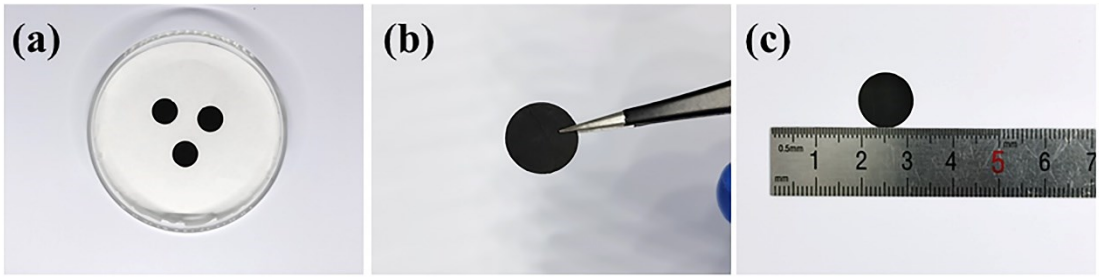

Fig. S13 1.5-ZnS@CNFs-800 composite are directly used as free-standing anodes for SIBs.

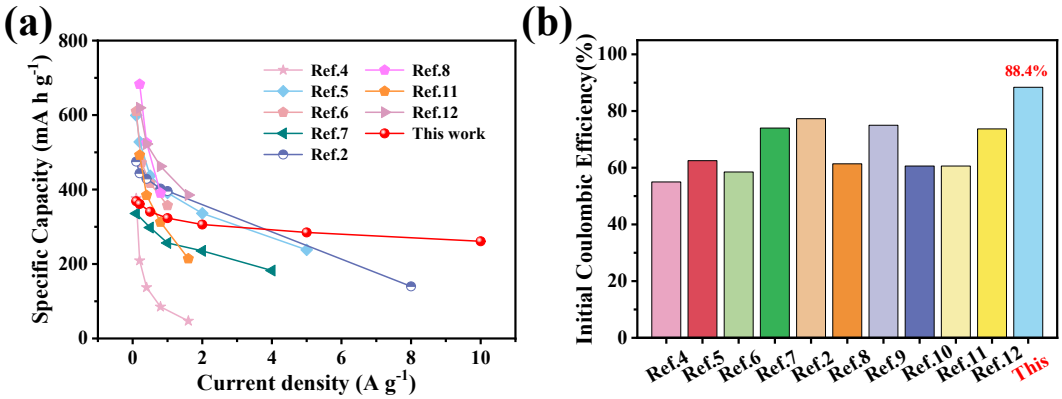

Fig. S14 (a) The Ragone plots of 1.5-ZnS@CNFs-800 and the reported ZnS-based anodes for SIBs. (b) Comparison of initial coulombic efficiency of 1.5-ZnS@CNFs-800 with those reported in the literatures.

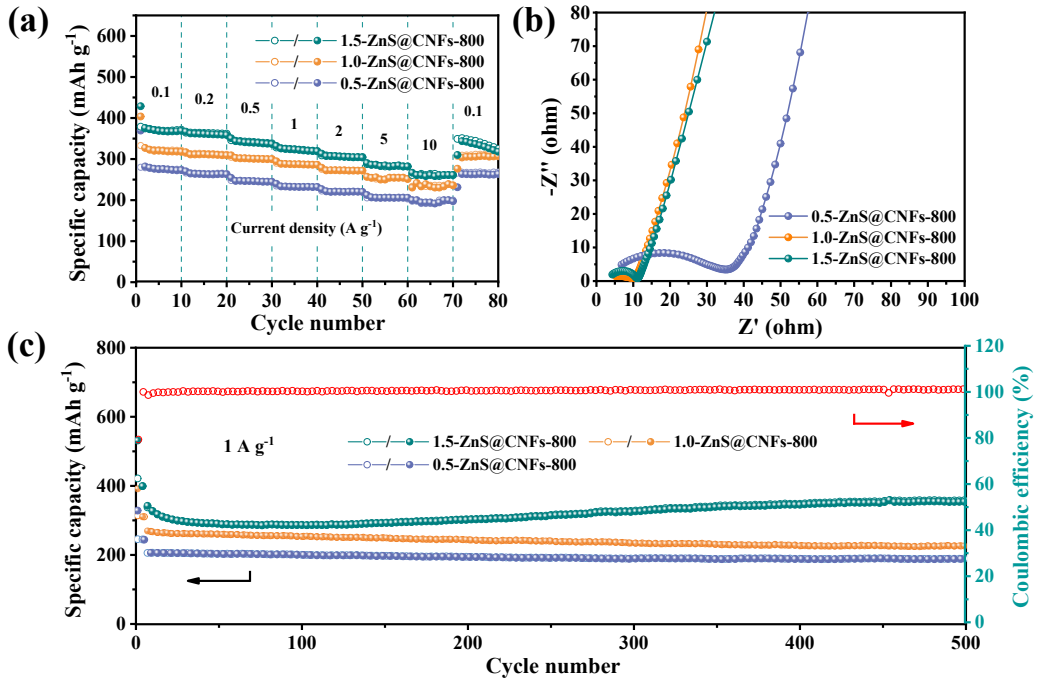

Fig. S15 Electrochemical properties of 0.5, 1.0, 1.5-ZnS@CNFs-800. (a) Rate performance, (b) Nyquist plots and (c) cycle performance of the three composites.

Due to the suitable carbonized temperature of 800 ℃, all the samples with different ZnS contents display outstanding rate performance and cycling stability. With the increasement of ZnS content, the carbon nanofibers possess much cavities, which could reduce the thickness of carbon shells, further shortening the distance of electron diffusion. Therefore, the 1.5-ZnS@CNFs-800 composite exhibit a relative low Rct. As to the small capacity increase of 1.5-ZnS@CNFs-800, it could be attributed to the smaller ZnS particles produced during cycling, which provide more active sites to obtain high specific capacity.

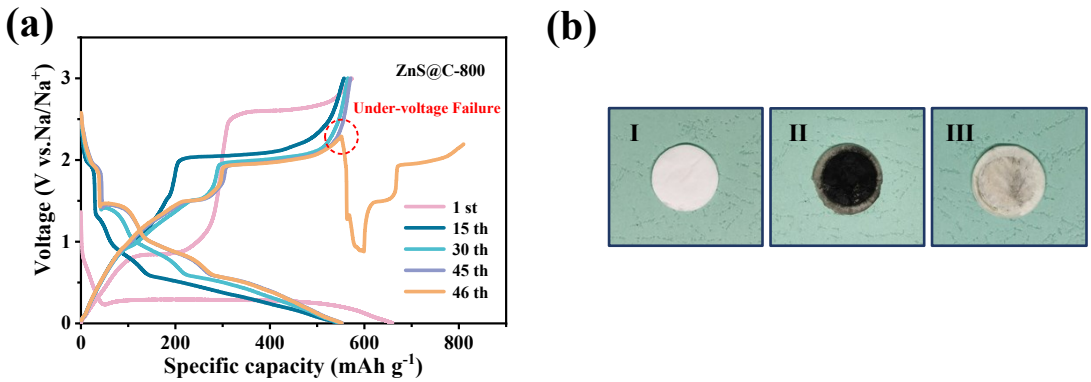

Fig. S16 (a) GCD profiles of ZnS@C-800 at 1 A g^{-1}. (b) Digital photographs of the separator from fresh (I), ZnS@C-800 failure cell (II) and 1.5-ZnS@CNFs-800 cell (III).

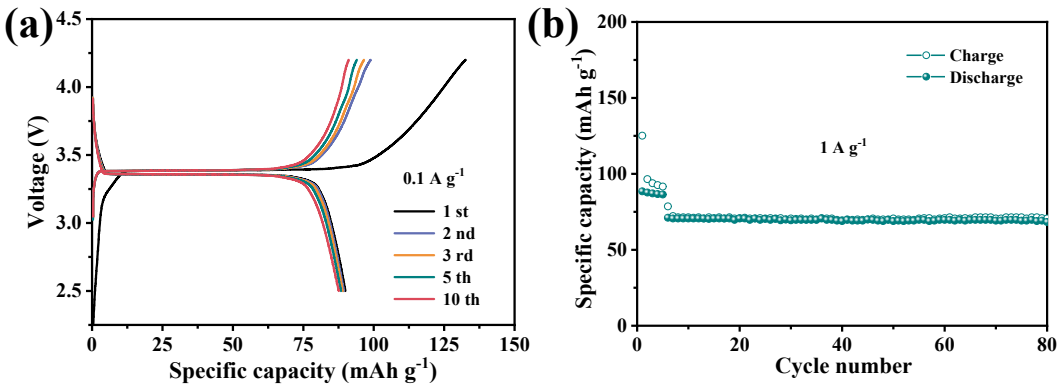

Fig. S17 Half-cell test of NVP cathode. (a) GCD curves and (b) cycling performance at 1 A g^{-1}.

The NVP half-cell presented excellent cycling stability under the currents of 0.1 A g^{-1} and 1 A g^{-1}, and a pre-sodiation procedure for 1.5-ZnS@CNFs-800 anodes were carried out to countervail the loss of sodium during the initial cycle in half-cells.

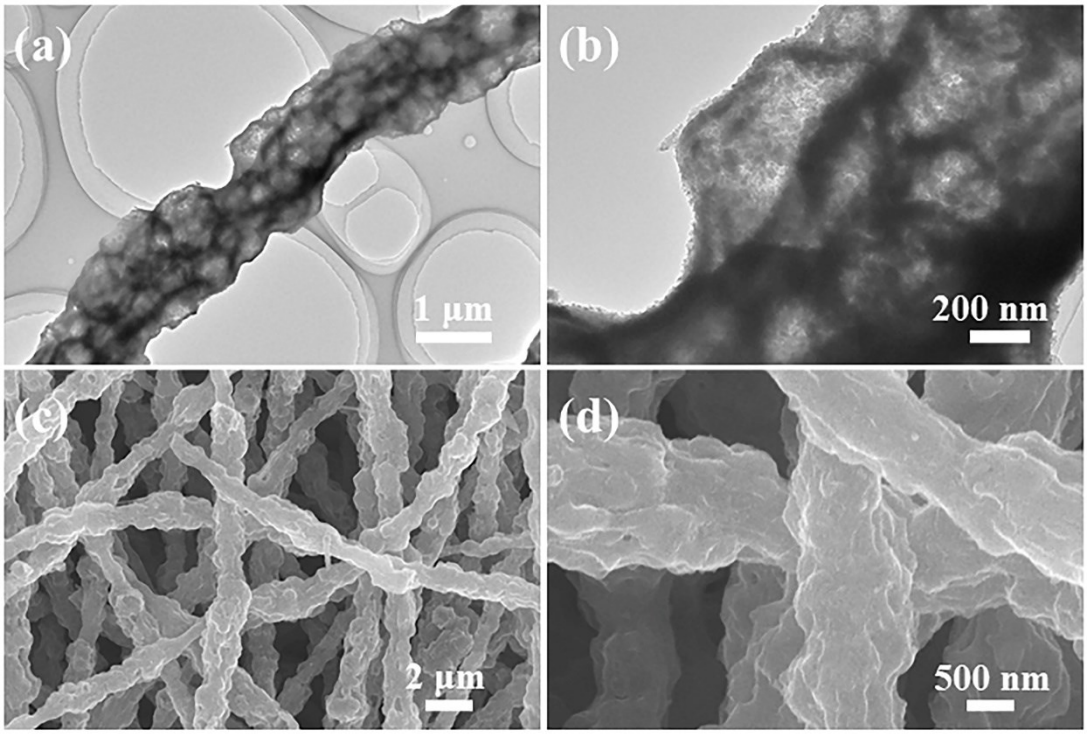

Fig. S18 (a, b) TEM images of 1.5-ZnS@CNFs-800 after 80 cycles at 0.2 A g^{-1} and the corresponding (c, d) SEM images.

Table S1. The content comparison (at %) of Zn, S, C, N and O elements for 1.5-ZnS@CNFs at different carbonization temperatures.

Sample	Zn	S	C	N	O
1.5-ZnS@CNFs-700	2.43	2.54	75.54	9.38	10.10
1.5-ZnS@CNFs-800	3.72	3.96	75.32	9.57	7.44
1.5-ZnS@CNFs-900	0.82	0.79	82.51	3.98	11.91

Table S2. The specific surface area and pore volume of different composites.

Sample	Specific Surface Area ($m^2\ g^{-1}$)	Pore Volume ($cm^3\ g^{-1}$))
CNFs-800	7.26	0.017
0.5-ZnS@CNFs-800	32.39	0.037
1.0-ZnS@CNFs-800	44.31	0.055
1.5-ZnS@CNFs-800	77.44	0.131

Table S3. The content comparison of different types of N in 1.5-ZnS@CNFs at different carbonization temperatures.

Sample	Oxide N (%)	Graphite N (%)	Pyrrolic N (%)	Pyridinic N (%)
1.5-ZnS@CNFs-700	4.4	31.1	11.8	53.7
1.5-ZnS@CNFs-800	8.6	25.1	12.4	53.9
1.5-ZnS@CNFs-900	8.5	37.6	7.2	46.7

Specifically, the total contents of pyrrolic N and pyridinic N in 1.5-ZnS@CNFs-800 is the highest among the three composites, which will contribute to a higher capacity.

Table S4. Sodium ion battery performance comparison of 1.5-ZnS@CNFs-800 with other reported ZnS-based anode materials.

Anode materials	ICE	Cycling number	Reversible Capacity (mAh g^{-1})	Rate capacity (mAh g^{-1})	Ref.
1.5-ZnS@CNFs-800 free-standing anode	88.4%	500	354.5 (1 A g^{-1})	323.8 (1 A g^{-1}) 307.2 (2 A g^{-1}) 283.3 (5 A g^{-1}) 258.3 (10 A g^{-1})	This work
m-ZnS NSs@NC	77.3%	300	370.3 (1 A g^{-1})	139.9 (8 A g^{-1})	[2]
ZnS nanoparticles / N doped C	55.2%	1000	289.2 (1 A g^{-1})	182.4 (4 A g^{-1})	[4]
ZnS nanoparticles / RGO	62.5%	50	481 (0.1 A g^{-1})	357 (1 A g^{-1})	[5]
ZnS quantum dots /RGO	58.5%	100	491 (0.1 A g^{-1})	317 (1 A g^{-1})	[6]
ZnS submicrospheres / C	74%	60	230 (0.1 A g^{-1})	47 (1.6 A g^{-1})	[7]
ZnS-Sb_2S_3@C	61.4%	120	630 (0.1 A g^{-1})	390.6 (0.8 A g^{-1})	[8]
ZnS-NC/SnS_2	75%	500	375.7 (1 A g^{-1})	405.9 (5 A g^{-1})	[9]
Hollow-SnS-ZnS@C@RGO	60.6%	1000	247 (2 A g^{-1})	348 (10 A g^{-1})	[10]
Mesoporous Sb/ZnS@C	60.6%	600	200 (1 A g^{-1})	214.3 (1.6 A g^{-1})	[11]
Co_3S_4-ZnS/NC	73.7%	200	619 (0.2 A g^{-1})	385.3 (1.6 A g^{-1})	[12]

References

1 N. L. Torad, M. Hu, Y. Kamachi, K. Takai, M. Imura, M. Naito and Y. Yamauchi, Facile synthesis of nanoporous carbons with controlled particle sizes by direct carbonization of monodispersed ZIF-8 crystals. *Chem Commun. (Camb)*, 2013, **49**, 2521-2523.

2 W. Ji, L. Hu, X. Hu, Y. Ding and Z. Wen, Nitrogen-doped carbon coating mesoporous ZnS nanospheres as high-performance anode material of sodium-ion batteries. *Mater. Today Commun.*, 2019, **19**, 396-401.

3 C. Yang, M. Zhang, N. Kong, J. Lan, Y. Yu and X. Yang, Self-supported carbon nanofiber films with high-level nitrogen and phosphorus co-doping for advanced lithium-ion and sodium-ion capacitors. *ACS Sustainable Chem. Eng.*, 2019, **7**, 9291-9300.

4 J. Li, D. Yan, X. Zhang, S. Hou, T. Lu, Y. Yao and L. Pan, ZnS nanoparticles decorated on nitrogen-doped porous carbon polyhedra: a promising anode material for lithium-ion and sodium-ion batteries. *J. Mater. Chem. A.*, 2017, **5**, 20428-20438.

5 W. Qin, D. Li, X. Zhang, D. Yan, B. Hu and L. Pan, ZnS nanoparticles embedded in reduced graphene oxide as high-performance anode material of sodium-ion batteries. *Electrochim. Acta*, 2016, **191**, 435-443.

6 R. Zhang, Y. Wang, M. Jia, J. Xu and E. Pan, One-pot hydrothermal synthesis of ZnS quantum dots/graphene hybrids as a dual anode for sodium ion and lithium ion batteries. *Appl. Surf. Sci.*, 2018, **437**, 375-383.

7 J. Ma, X. Wang, H. Wang, G. Wang and S. Ma, Hollow ZnS submicrospheres encapsulated in carbon shells with enhanced lithium and sodium storage properties. *J. Alloy. Compd.*, 2018, **735**, 51-61.

8 S. Dong, C. Li, X. Ge, Z. Li, X. Miao and L. Yin, ZnS-Sb_2S_3@C core-double shell polyhedron structure derived from metal-organic framework as anodes for high performance sodium ion batteries. *ACS Nano*, 2017, **11**, 6474-6482.

9 J. Yuan, B. Qu, Q. Zhang, W. He, Q. Xie and D. L. Peng, Ion reservoir enabled by hierarchical bimetallic sulfides nanocages toward highly effective sodium storage. *Small*, 2020, **16**, 1907261.

10 Y. Zhang, P. Wang, Y. Yin, X. Zhang, L. Fan, N. Zhang and K. Sun, Heterostructured SnS-ZnS@C hollow nanoboxes embedded in graphene for high performance lithium and sodium ion batteries. *Chem. Eng. J.*, 2019, **356**, 1042-1051.

11 S. Dong, C. Li, Z. Li, L. Zhang and L. Yin, Mesoporous hollow Sb/ZnS@C core-shell heterostructures as anodes for high-performance sodium-ion batteries. *Small*, 2018, **14**, 1704517.

12 Z. Zhang, Y. Huang, X. Liu, C. Chen, Z. Xu and P. Liu, Zeolitic imidazolate frameworks derived ZnS/Co_3S_4 composite nanoparticles doping on polyhedral carbon framework for efficient lithium/sodium storage anode materials. *Carbon*, 2020, **157**, 244-254.